

Low dimensional correlations under thermal fluctuations

N. Kestn¹ and T. Giamarchi¹

¹*Department of Quantum Matter Physics, University of Geneva, 1211 Geneva, Switzerland*

(Dated: December 15, 2024)

We study the correlation functions of quantum spin 1/2 ladders at finite temperature, under a magnetic field, in the gapless phase at various relevant temperatures $T \neq 0$, momentum q and frequencies ω . We compute those quantities using the time dependent density matrix renormalization group (T-DMRG) in some optimal numerical scheme. We compare these correlations with the ones of dimerized quantum spin chains and simple spin chains, that we compute by a similar technique. We analyze the intermediate energy modes and show that the effect of temperature lead to the formation of an essentially dispersive mode corresponding to the propagation of a triplet mode in an incoherent background, with a dispersion quite different from the one occurring at very low temperatures. We compare the low energy part of the spectrum with the predictions of the Tomonaga-Luttinger liquid field theory at finite temperature. We shows that the field theory describes in a remarkably robust way the low energy correlations for frequencies or temperatures up to the natural cutoff (the effective dispersion) of the system. We discuss how our results could be tested in e.g. neutron scattering experiments.

I. INTRODUCTION

The study of strongly correlated system is of crucial importance for both the cold atom and the condensed matter communities. In particular, both are able to provide experimental realizations with well controlled microscopic Hamiltonians either using optical lattices^{1,2} or quantum magnets.³ On the theory side, going from the knowledge of the microscopic Hamiltonian to the calculation of the correlations, which can be confronted to experimental measurements, is of course a considerable challenge.

One class of systems which presents a very rich set of phases, depending on the precise microscopic interactions is the one of quantum one- or quasi-one dimensional magnets.⁴ Indeed such systems possess ground states ranging from quasi-long range magnetic order to spin liquids. The coupling of several one-dimensional chains as ladders leads to a very rich phase diagram as a functions of the number of legs.⁵ The correlations in these systems can be probed by e.g. inelastic neutron scattering (INS)⁶ or nuclear magnetic resonance (NMR)⁷ experiments, giving a very complete access to the spatial or time dependence of the spin-spin correlations.

In such systems the precise knowledge of the microscopic Hamiltonian allows thus for a drastic test of the theoretical methods used to compute the correlations. However computing the correlation analytically, by methods such as Bethe-Ansatz⁸ has only proven possible at zero temperature. Comparison with experiments could thus be done for probes, such as neutrons, when the energy of the probe is much larger than the temperature.^{9,10} Numerical methods, such as the Density Matrix Renormalization Group (DMRG)^{11–17} allowed for a direct calculation of the zero temperature correlations that could be successfully compared with experiments for ladder systems.^{18,19}

An important challenge is of course to properly incorporate the finite temperature effects. For temperatures

much lower than the magnetic exchanges in the problem this can be accomplished by using a combination of the field theory description, such as the Tomonaga-Luttinger liquid (TLL) theory⁴ and numerics to get an essentially quantitative finite temperature description, which could be successfully confronted with experiments.^{18,20,21} However this description breaks down when the temperature becomes comparable with the exchanges or close to a quantum critical point (QCP)^{22,23} and it is desirable to have a direct way to quantitatively compute the correlations at finite temperature.

Fortunately such a method is provided by the DMRG, which can be used to compute the finite temperature dynamical correlations at the expense of much more heavy calculations.^{24–27} This program has been carried out with success for spin 1/2 chains²⁸ where it allowed in particular to analyze the surrounding of the quantum critical point close to saturation and neutron experiments.²⁹ Spin-one single-ion anisotropy^{30,31} and dimerized chains³² could be analyzed at finite temperature. For the dimers both NMR³³ and the neutron scattering³⁴ could be computed allowing to investigate the broadening effects due to the temperature on the spectrum.³⁵

We investigate in the present paper the thermal effects on the spin-spin correlations of a ladder system. On the theory side this allows for a comparison between the ladder and dimerized systems. On the more experimental one this is stimulated by recent experiments done in ladders which were done close to a quantum critical point³⁶ or the existence of compounds with relatively small magnetic exchange such as the bis-piperidinium copper tetrachloride (BPCC)³⁷ for which we can expect the effects of temperature to be a priori more important. On the technical point of view the ladders are more challenging due to the greater entanglement compared to either spin chains and dimers. In this paper we will mostly focus on the comparison of the thermal effects between the ladders, dimers and chains. We also compare the direct nu-

merical calculations with the field theory description at finite temperature in order to have a feeling of the range of validity of the field theory description, in a spirit similar to what was done previously for NMR.³⁴

The plan of the paper is as follows. In Sec. II, we introduce the low dimensional models that we will study during the whole paper. We then explain details about the numerical algorithm for the measure of the low dimensional correlations in Sec. III. We then move forward and present the dynamical structure factors IV of the various models at different temperature that inelastic neutron scattering experiment can measure also. We finally compare the low energy spectrum with some analytical field theory in Sec. V and discuss the deviation from bosonization expectations.

II. MODELS

In this work, we focus on three classes of problems made of coupled spin 1/2, namely: i) ladder systems \mathcal{L} made of two coupled spin chains; ii) weakly dimerized chains \mathcal{D} ; iii) $\Delta = \frac{1}{2}$ anisotropic XXZ chains \mathcal{C} .

1. Ladder \mathcal{L}

We consider a two leg ladder system with spin 1/2 coupled by anti-ferromagnetic Heisenberg couplings on rungs and legs (see Fig. 1)

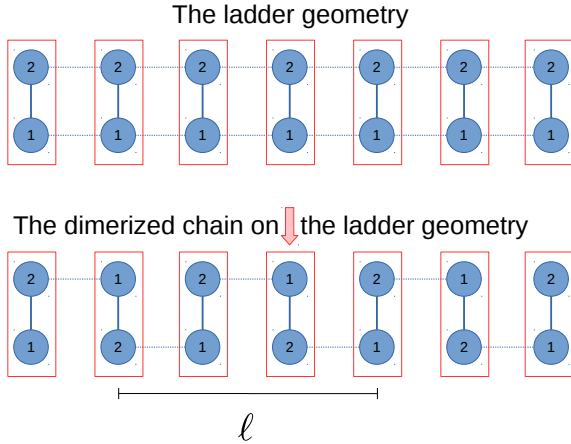


FIG. 1. Weakly coupled dimer and ladder representation. The index η corresponds for the ladder to the bottom or upper leg. For the dimer, η corresponds to the left or right strong bond cell, thus the labels shuffle when mapped on the ladder geometry. We add an arrow on the middle cell to visualize the symmetry when we inverse the dimerized chain.

$$H_{\mathcal{L}} = J_{\parallel} \sum_{\ell, \eta} \mathbf{S}_{\ell, \eta} \cdot \mathbf{S}_{\ell+1, \eta} + J_{\perp} \sum_{\ell} \mathbf{S}_{\ell, 1} \cdot \mathbf{S}_{\ell, 2} - h^z \sum_{\ell, \eta} S_{\ell, \eta}^z \quad (1)$$

with stronger rung coupling where $\mathbf{S}_{\ell, \eta}$ denotes a spin 1/2 at rung ℓ on leg $\eta \in \{1, 2\}$. The spin-half $\mathbf{S} = (S^x, S^y, S^z) = \frac{\hbar}{2}(\sigma^1, \sigma^2, \sigma^3)$ can be decomposed in lowering and raising operators $S^{\pm} = S^x \pm iS^y$, where we denote by σ^i the Pauli matrices, $i \in \{1, 2, 3\}$.

2. Dimer \mathcal{D}

If we remove alternatively the weak bonds along the ladder (see Fig. 1) and map the model to a chain we get a dimerized chain of alternative bonds. For an even number of site N , we always have $\frac{N}{2}$ strong bonds J_s and $\frac{N}{2} - 1$ weak bonds J_w . The model is thus

$$H_{\mathcal{D}} = \sum_{n=1}^{N-1} (J - (-1)^n \delta J) \mathbf{S}_n \cdot \mathbf{S}_{n+1} - h^z \sum_{n=1}^N S_n^z \quad (2)$$

starting with a strong bond at each border.

3. Spin-Chain mapping - $\Delta = \frac{1}{2}$ XXZ chain \mathcal{C}

Both previous models can be mapped to an anisotropic single spin-chain in some regime of parameters when studying the low energy behavior.¹⁸ If the magnetic field and temperature is such that we neglect the triplet $|t^0\rangle$ and $|t^-\rangle$ population, one can identify a spin-chain behavior in the critical interplay between $|t^+\rangle$ and $|s\rangle$.

We introduce the pseudo spin-half \vec{S} in the basis $|\uparrow\rangle \equiv |t^+\rangle$, $|\downarrow\rangle \equiv |s\rangle$ mapped by $S_{\eta}^{\pm} \equiv \frac{\eta}{\sqrt{2}} S^{\pm}$ and $S_{\eta}^z \equiv \frac{1}{4}(1 + 2S^z)$ in the singlet-triplet crossing region. The mapping leads to a spin-half XXZ chain with $\Delta = \frac{1}{2}$ anisotropy

$$H_{\mathcal{C}} = J \sum_{\ell=1}^{N-1} \left(S_{\ell}^x S_{\ell+1}^x + S_{\ell}^y S_{\ell+1}^y + \frac{1}{2} S_{\ell}^z S_{\ell+1}^z \right) - h_{eff}^z \sum_{\ell=1}^N S_{\ell}^z \quad (3)$$

The spin-chain mapping fixes the following microscopic parameters for the XXZ model

- ladder : $J \equiv J_{\parallel}$ and $h_{eff}^z = h^z - J_{\perp} - \frac{J_{\parallel}}{2}$.
- dimer : $J \equiv -\frac{J_w}{2}$ and $h_{eff}^z = h^z - J_s - \frac{J_w}{4}$.

Although these models can be studied independently we consider them here in the regime where their low energy properties are roughly equivalent. We consider spin chains close to zero magnetization $m_{\mathcal{L}} = 0$, which means that both the ladder and the dimer are at a magnetization around half saturation $m_{\mathcal{L}} = 0.5$ and $m_{\mathcal{D}} = 0.25$ at $T = 0$. We call this point in the paper the **studied magnetic point** for simplicity.

For the numerical study we fix the ratio of coupling constants of the ladder to values corresponding roughly to the compound BPCC^{37–40} namely

$$\begin{aligned} J_{\perp} &= 1 \\ J_{\parallel} &= 0.39 J_{\perp} \end{aligned} \quad (4)$$

In the same way for the dimer system we have

$$\begin{aligned} J_w &= J - \delta J = 0.39 J_s \\ J_s &= J + \delta J = 1 \end{aligned} \quad (5)$$

The corresponding values for the magnetic field are respectively $h^z \simeq 1.28 J_\perp$ for the ladder and $h^z \simeq 1.148 J_s$ for the dimer. We will consider these values in the rest of the manuscript. We will not discuss the correction of the constant and the boundary terms in this work.

One can see how the spin-chain mapping manifests on both models looking at Figs. 3 and 4 compared with Figs. 5 and 6.

III. METHOD T-DMRG ($T \neq 0$)

We implement in this paper a time dependent density matrix renormalization group (T-DMRG) procedure,^{24–27} a method based on the earlier DMRG algorithm.^{11–17}

The method is schematically represented in Fig. 2. The time or imaginary time evolution follows the Suzuki-Trotter decomposition.^{41,42} In this work we used a fourth-order decomposition – that expands the exponentials in terms of gates which now can converge to the thermal equilibrium function $\frac{1}{Z}e^{-\beta H}$. One introduces hierarchical matrices for tensors that increases the amount of information stored in the system based on the local quantum numbers^{43,44} and the global conservation rules.

Both DMRG and T-DMRG algorithm have the same complexity limit in term of the bond dimension χ of the matrices – during updates after application of above-mentioned gates. Naively the singular value decomposition scales¹⁵ as $O(\chi) \sim A\chi^3$ but with different prefactors A which increases from d^3 for DMRG to d^6 for T-DMRG, where d is the number of local degrees of freedom. A similar scaling applies to the memory where $O(\chi) \sim A\chi^2$ with $A \propto d^2$ for DMRG and $A \propto d^4$ for T-DMRG. For the case of ladders, due to the effective longer range of the couplings, if one represents the system as a chain, the gates have to be applied further which increases further the complexity. This is related to the fact that DMRG is most efficient for quantum problems with sufficiently low amount of relevant information⁴⁵ and thus particularly to the low dimensional problems.

A. T-DMRG and a close to optimal scheme

Since the complexity of the ladder and of the dimer is different due to the longer range of the coupling (see Fig. 1), one needs to restrict the bond dimension χ according to the problem. We use in this work values of χ of the order of $\chi_{\mathcal{L}} \sim 620$ for the ladders and $\chi_{\mathcal{D}} \sim 2400$ for the dimers.

With the values of $\chi_{\mathcal{L}}$ for the ladders, the use of the standard scheme^{27,34} of implementation of the

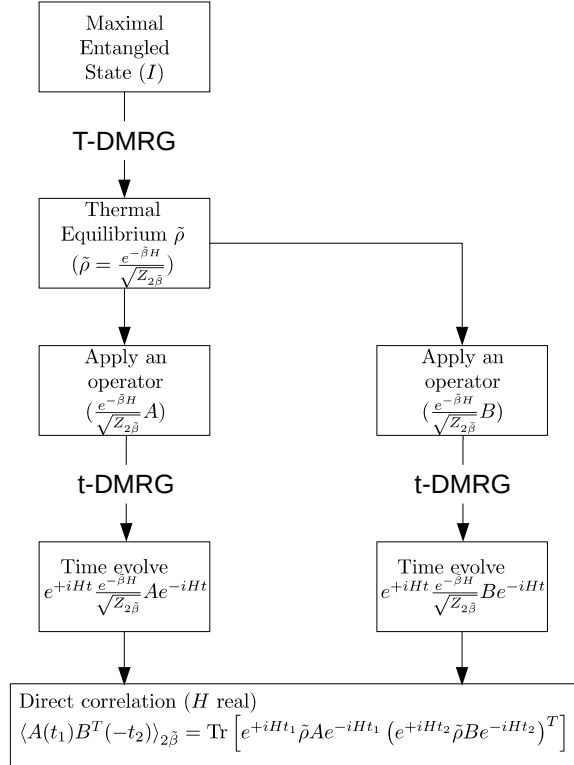


FIG. 2. Simulation and measurement of direct correlations by evolving in time two observables to t_1 and t_2 at finite temperature using the T-DMRG algorithm. An optimal scheme, explained in Ref. 27, consists in evolving separately the two observables. This scheme requires storing all intermediate steps and contracting them at the end (see text). We use this scheme for the ladders since it can in principle double the resolution. The standard scheme consists in evolving only one observable in time ($t_2 = 0$) and in the present paper we use it both for the dimers and the chains. Please note, that in our notation $\beta = 2\tilde{\beta}$.

time/temperature evolution does not allow to reach sufficiently long time and resolution for the ladder case. This happens even though the dimers and ladders look naively quite similar. Thus in order to be able to study reliably the ladders we have implemented an optimal numerical scheme as described in Ref. 27 (see Fig. 2), which was only scarcely used in the literature previously due to its more demanding implementation. As shown in Fig. 2, the usual procedure is evolving in time only one observable, while the optimal scheme consists of evolving both operators in time. In practice, this requires only logistic (storing of the state) and running the jobs in parallel.⁴⁶ But due to hardware limits, it is in practice difficult to store all the states and parallelize the contraction properly.

We use the optimal scheme for the ladder case to in-

TABLE I. Temperature presented in the following picture. All the results are given at the *studied magnetic point* in the middle of the critical gapless phase.

Model	Figure	Temperature
ladder \mathcal{L}	Fig. 3	$T \simeq 0.25 J_{\perp} \simeq 0.64 J_{\parallel}$
	Fig. 4	$T \simeq 0.595 J_{\perp} \simeq 1.526 J_{\parallel}$
dimer \mathcal{D}	Fig. 5	$T \simeq 0.25 J_s \simeq 1.28 J_w/2$
	Fig. 6	$T \simeq 0.595 J_s \simeq 3.05 J_w/2$
chain \mathcal{C}	Fig. 7	$T \simeq 0.25 J$

crease the resolution of Fig. 3 and Fig. 4. For the other models, we use the normal scheme consisting of evolving only one observable in time (Fig. 2 with $t_2 = 0$).

We compute the spin-spin correlations in space and time

$$\langle S_{x_0}^{\alpha}(t) S_{x_1}^{\gamma} \rangle_{\beta} \quad (6)$$

for positive time $t \geq 0$ and fixed observable at x_0 . We detail in Sec. IV below how we Fourier transform the measured correlations. We compute these correlations for various temperatures as given in Table I.

B. Simulation accuracy

Comparing the initial DMRG version with the finite temperature algorithm, one sees that the variance of the Hamiltonian $\langle (H - \langle H \rangle)^2 \rangle$ is now finite and no longer a criterion for convergence. To define the convergence of the calculation, we use the discarded weight quantity,²⁷ namely the total weight of discarded eigenvalues according to the singular value λ_j decomposition.

$$\epsilon_i \equiv \left(\frac{\|X_{\text{trunc}} - X\|}{\|X\|} \right)^2 = \frac{\sum_{j>\chi} \lambda_j^2}{\sum_j \lambda_j^2} \quad (7)$$

where i can denote the inverse temperature β , the time t or a single step process depending on the context. The sum applies in all quantum sector blocks. X is in the matrix product operator²⁴ form and X_{trunc} is the truncated matrix product approximation with the renormalized bond dimension fixed to χ .

The norm can be viewed as the Frobenius norm.²⁷ χ is the bond dimension of the mixed state, and corresponds to the number of states kept in the system. This discarded weight quantity is a good indicator of the T-DMRG algorithm precision (see Appendix C).

1. Ladders \mathcal{L}

For the ladder, we fixed the size to a total of $45 \cdot 2 = 90$ ladder sites. The run uses a truncation error $\epsilon_{\beta} =$

10^{-18} and steps in imaginary time $\delta\beta = \frac{1}{100}$ to converge to the thermal equilibrium $\beta = 4.0 J_{\perp}^{-1}$, $3.04 J_{\perp}^{-1}$ and $1.68 J_{\perp}^{-1}$ which are the three temperatures considered for the ladders in the present paper.

The initial bond dimension $\chi_{\beta} < 800$ remains largely controlled (it did not reach the limit size 800) in this initial step since the temperatures are quite large. Once then we fix for all the different observable the truncation $\epsilon_t = 10^{-13}$, $\delta t = \frac{1}{16}$ and bond dimension $\chi_t = 620$. Typically the amount of information in the time simulation grows until the maximal bond dimension is reached. Then, one loose a precision of ϵ_i at each step by throwing the smallest singular values λ_j according to (7). It is mandatory if one wants to keep the numerical algorithmic complexity size χ of the matrices fixed. The algorithm stops when the total discarded weight pass a threshold $\sum_{i \in \{\text{all steps}\}} \epsilon_i > 10^{-2}$ or when a single step lacks in precision $\epsilon_i > 10^{-5}$.

The above precision is for the middle site observable (left column of Fig. 2). All the other observables run in parallel with the same time algorithm procedure (or half the sites using afterwards the symmetry along the ladder). In order to be sufficiently fast, we reduce the bond dimension $\chi_t = 400$ as well as the final time $t_2 \sim 7-8 J_{\perp}^{-1}$ to insure a precision $\epsilon_t \lesssim 10^{-7}$. We can then compute the direct correlations in Fig. 2 with t_1 up to $19-23 J_{\perp}^{-1}$ and we find a good overlap between all different time correlations – it get a bit worse for values of t_1 close to the maximal reachable time as expected. This optimal scheme brings an increase in time $t = t_1 + |t_2|$ or a resolution improvement of $\sim 30-50\%$ in the worst or best scenario.

2. Dimers \mathcal{D}

For the dimer case, we get a similar resolution in J_s without using the optimal scheme for $L = 90$ sites. We first converge with the truncation error $\epsilon_{\beta} = 10^{-18}$ with steps $\delta\beta = \frac{1}{100}$ to the thermal equilibrium at $\beta = 20 J_{\perp}^{-1}$, $10 J_{\perp}^{-1}$, $4.0 J_{\perp}^{-1}$, $1.68 J_{\perp}^{-1}$. One then fix all the different observables and time evolve by $\delta t = \frac{1}{16}$ with the truncation $\epsilon_t = 10^{-13}$ with the limited bond $\chi_t = 2400$. The simulation stops again according to the same threshold and the final times are for the high temperatures of order $t_{\text{max}} \sim 27-36 J_{\perp}^{-1}$. For a lower temperature $T \ll J_w$, one can achieve a better resolution similar to standard DMRG results (see 34).

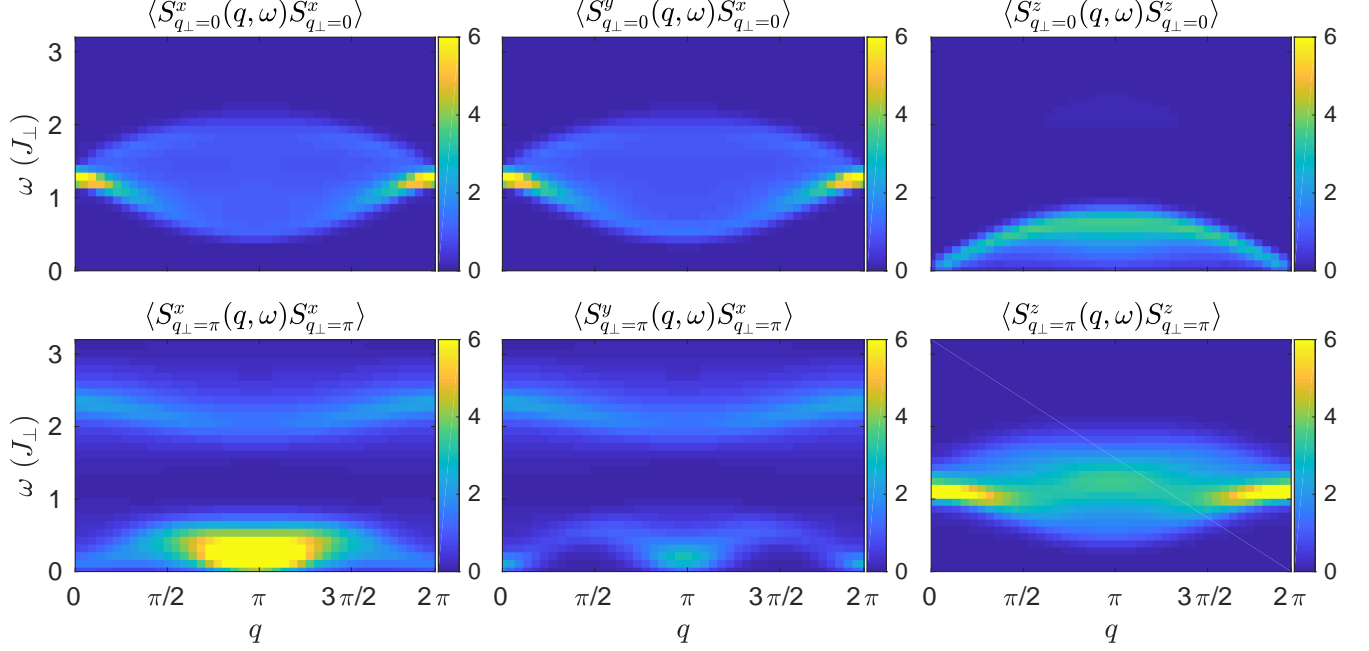


FIG. 3. Spin-spin correlations of a spin 1/2 ladder in units of $J_{\perp} = 1$ with $J_{\parallel} = 0.39 J_{\perp}$ at $T = 0.25 J_{\perp}$ for magnetic field $h^z \simeq 1.28 J_{\perp}$ corresponding to $m_{\mathcal{L}} = 0.5$. The resolution is $\delta\omega = \frac{\pi}{30 J_{\perp}^{-1}}$ using the optimal scheme.

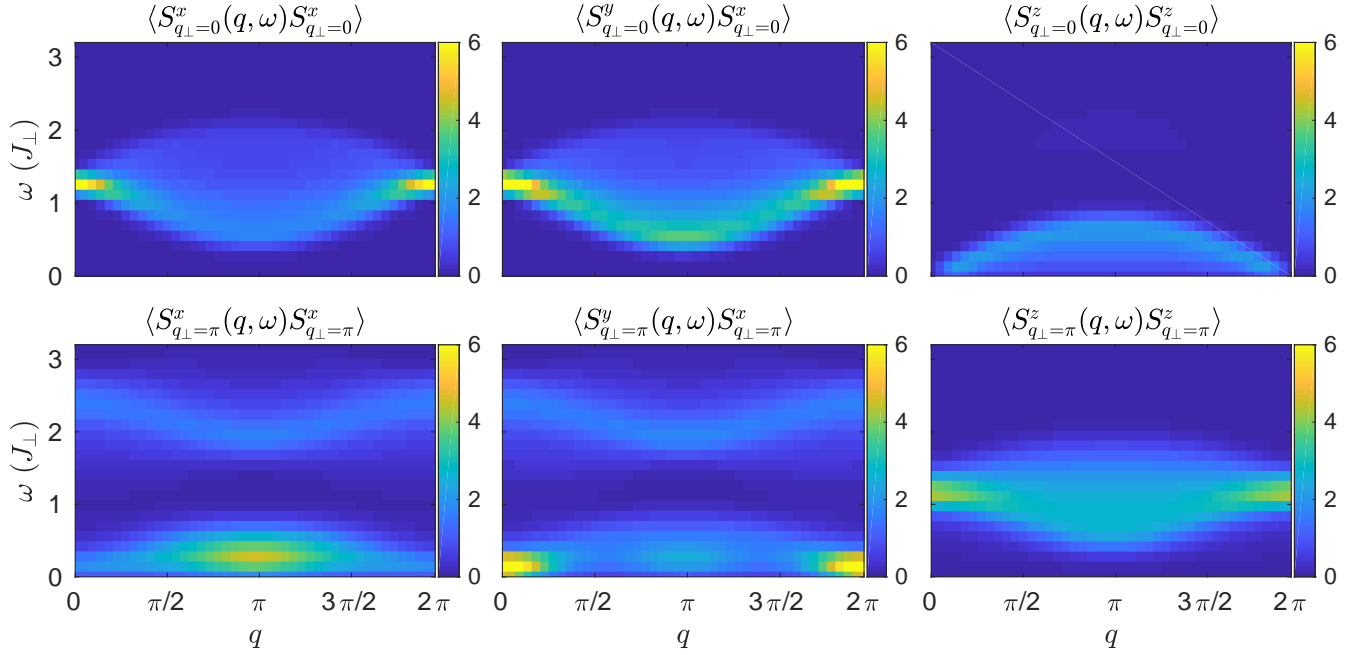


FIG. 4. Spin-spin correlations of a spin 1/2 ladder in units of $J_{\perp} = 1$ with $J_{\parallel} = 0.39 J_{\perp}$ and at $T \simeq 0.59 J_{\perp}$ for magnetic field $h^z \simeq 1.28 J_{\perp}$ corresponding to $m_{\mathcal{L}} = 0.5$. The resolution is $\delta\omega = \frac{\pi}{22.5 J_{\perp}^{-1}}$ using the optimal scheme.

IV. CORRELATIONS FOR LADDERS, DIMERS AND CHAINS

A. Dynamical structure factor

We first need to transform the real time and space data to find the dynamical structure factor.

$$S^{\alpha\gamma}(\mathbf{q}, \omega) = \int_{-\infty}^{\infty} d\mathbf{r} dt e^{i(\omega t - \mathbf{q} \cdot \mathbf{r})} \langle S^{\alpha}(\mathbf{r}, t) S^{\gamma}(0, 0) \rangle \quad (8)$$

In the following equations, $\alpha, \gamma \in \{x, y, z, \pm\}$ denote any component of the spin 1/2.

The T-DMRG simulation gives the direct correlations $\langle S_{x_0}^{\alpha}(t) S_{x_1}^{\gamma} \rangle_{\beta}$ restricted to positive time $t \geq 0$. In order to avoid making errors using spatial invariance too early (before time inversion which can be critical for dimers) we use the retarded susceptibility to insure an exact procedure. Although this sounds a priori more complicated, it actually becomes more straightforward since the time symmetry is carried by the Kramers-Kronig relations. Furthermore, the S^z sector of the spin does not need the average magnetization – hidden in the real part – to calculate the connected correlation.

1. Chains \mathcal{C}

We illustrate this procedure for the spin chain. We first Fourier transform in time the retarded susceptibility that we get by expressing it in function of our direct correlations

$$\begin{aligned} \chi_{\text{ret}}^{\alpha\gamma}(\omega, x_0, x_1) &= \int dt e^{+i(\omega + i\varepsilon)t} (-i\Theta(t)) \langle [S_{x_0}^{\alpha}(t), S_{x_1}^{\gamma}] \rangle \\ &= -i \int_0^{+\infty} dt e^{+i(\omega + i\varepsilon)t} \left(\langle S_{x_0}^{\alpha}(t) S_{x_1}^{\gamma} \rangle - \overline{\langle S_{x_0}^{\alpha\dagger}(t) S_{x_1}^{\gamma\dagger} \rangle} \right) \end{aligned}$$

where $\overline{\langle \dots \rangle}$ denotes complex number conjugation and $S_{x_0}^{\pm\dagger} = S_{x_0}^{\mp}$. We then use translation invariance $x = x_1 - x_0$ in the bulk and Fourier transform the space

$$\chi_{\text{ret}}^{\alpha\gamma}(q, \omega) = \int dx e^{-iqx} \chi_{\text{ret}}^{\alpha\gamma}(\omega, x)$$

to finally get the dynamical structure factor worked out using the Lehmann representation

$$S^{\alpha\gamma}(q, \omega) = \frac{-2}{1 - e^{-\beta\omega}} \text{Im}(\chi_{\text{ret}}^{\alpha\gamma}(q, \omega))$$

The detail of this equality can be found in Appendix D.

2. Ladders \mathcal{L}

For the ladder, we have two species of correlations according to the leg index $\eta \in \{1, 2\}$. We use the q_{\perp} momentum to represent the correlations since it is a good

quantum number. Thereby the observables and correlations separate in the symmetric $q_{\perp} = 0$ or anti-symmetric $q_{\perp} = \pi$ sectors. We use the following definitions

$$\begin{aligned} S_{\ell, q_{\perp}=0}^{\alpha} &\equiv S_{\ell, 1}^{\alpha} + S_{\ell, 2}^{\alpha} \\ S_{\ell, q_{\perp}=\pi}^{\alpha} &\equiv S_{\ell, 1}^{\alpha} - S_{\ell, 2}^{\alpha} \end{aligned}$$

and calculate the dynamical structure factor from there. The two correlations are fully represented in the two q_{\perp} quantum sectors

$$\langle S_{q_{\perp}}^{\alpha}(q, \omega) S_{q_{\perp}}^{\gamma} \rangle = 2 (\langle S_1^{\alpha}(q, \omega) S_1^{\gamma} \rangle \pm \langle S_1^{\alpha}(q, \omega) S_2^{\gamma} \rangle)$$

where the index corresponds to correlations on same legs or respectively different legs. The symmetric $q_{\perp} = 0$ case corresponds to the sum while the anti-symmetric $q_{\perp} = \pi$ is the difference. Using the rung symmetry, all other mixture vanish $\langle S_{q_{\perp}=0}^{\alpha}(q, \omega) S_{q_{\perp}=\pi}^{\gamma} \rangle = 0$.

3. Dimers \mathcal{D}

Dimers have less symmetries than the ladder. One can map the dimer on the ladder structure, but q_{\perp} is not a good quantum number anymore. This can be seen for the $\langle S_{\ell, 1}^{\alpha} S_{0, 2}^{\gamma} \rangle$ correlation which is not symmetric by space inversion anymore – contrarily to the ladder case (see Appendix B). In one direction the correlation starts with a weak bond while in the other direction it starts with a strong bond. However, we can map the dimer on the ladder by introducing similar definitions

$$\begin{aligned} S_{\ell, q_{\perp}=0}^{\alpha} &\equiv (S_{\ell, 1}^{\alpha} + S_{\ell, 2}^{\alpha}) \\ S_{\ell, q_{\perp}=\pi}^{\alpha} &\equiv (S_{\ell, 1}^{\alpha} - S_{\ell, 2}^{\alpha})(-1)^{\ell} \end{aligned}$$

The new ladder labeling introduces oscillating sign according to Fig. 1 while the symmetric observable $S_{\ell, q_{\perp}=0}^{\alpha}$ remains untouched by the permutation. Note that the crossed correlations $\langle S_{q_{\perp}=0}^{\alpha}(q, \omega) S_{q_{\perp}=\pi}^{\gamma} \rangle \neq 0$ are not vanishing but not very transparent to analyze. We thus focus on the correlations

$$\begin{aligned} &\langle S_{q_{\perp}=0}^{\alpha}(q, \omega) S_{q_{\perp}=0}^{\gamma} \rangle \\ &\langle S_{q_{\perp}=\pi}^{\alpha}(q, \omega) S_{q_{\perp}=\pi}^{\gamma} \rangle \end{aligned}$$

These correlations looks similar to the ladder up to finite signal strength absent in the ladders as can be seen in Fig. 5 and Fig. 6.

For completeness, we also present in Appendix A (Fig. 12) the results in the more conventional chain notation in which we separate the correlations in $\langle S_1^{\alpha}(q, \omega) S_1^{\gamma} \rangle$ and $\langle S_1^{\alpha}(q, \omega) S_2^{\gamma} \rangle$ which are now 2 sites cell translation invariant.

4. Filter

Each Fourier transform leads to finite size effects. In the first part IV B, we add a weak gaussian filter

$M(x, t) = e^{-(Ax/d_{max})^2} e^{-(Bt/t_{max})^2}$ where we choose $A = B = 1.5$. In the second part V, where we compare the results with the field theory expectation, we avoid all filters and worked with the raw correlations.

B. Results for the correlation functions

Let us now present the results based on the calculations described in the previous sections.

The central results of this section are the calculation of the correlation functions for the ladders at finite temperature. Results for the ladder model (1) are presented in Fig. 3 for a temperature of $T = 0.25 J_\perp$ and in Fig. 4 for temperature $T \simeq 0.59 J_\perp$.

In the same way, and in order to be able to compare with the ladder results we present the finite temperature correlations for the dimerized system. Similar calculations, albeit at different temperatures and couplings were given in Ref. 34. The comparison of the results of the present paper with the results of Ref. 34 for the correlation $\langle S_1^\alpha S_1^\gamma \rangle_\beta$ in the gapless phase is very good. We find similar limitations during time evolution process for the most cumbersome $\frac{e^{-\beta H}}{Z} S^+$ observable and similar improvement of resolution when lowering the temperature.

The dimerized system mapped on the ladder geometry is shown in Fig. 5 at a temperature $T = 0.25 J_s$ and in Fig. 6 for a temperature $T \simeq 0.59 J_s$.

Finally we also present the results for the chains at identical temperature in Fig. 7. Finite temperature calculations of spin chains were also presented in Ref. 28.

C. Discussion of the T-DMRG results

First let us note that the weights in the correlations redistribute differently than for zero temperature case.¹⁸ Due to the finite temperature effects, some negative energy transitions are allowed in the correlations (see Fig. 12). We only present the results for the positive frequency domain $\omega \geq 0$ since one can relates them to the negative frequencies using the detailed balance equation (D3)

$$S^{\alpha\gamma}(q, \omega) = e^{-\beta\omega} S^{\gamma\alpha}(-q, -\omega) \quad (9)$$

Since the raising and lowering are not self conjugate operators, they are allowed at finite temperature to get negative intensities (see Fig. 12).

Even though the nature of the correlations are quite different due to the different species of correlations, ladders and dimers are quite related and gives good information on each other. There are indeed many similarities in the structure factor. The triplets are quite well aligned in energy. One difference that can be directly seen in the numerical results but will be deepened using the mapping onto an effective spin chain (see Sec. V C) is that

the dimer has an effective dispersion of $J_w/2$ compared to J_\parallel for the ladder. All quantities depending on the weak bonds thus rescale for the dimer by a factor of two. For this reason, we use a twice bigger colorbar color code for the dimer than the ladder to represent the intensities on a similar scale – but all presented results stay in unity of J_s and J_\perp . In addition, due to the asymmetry of the dimer, some signal survive in the region where the ladder is actually gapped (correlations in $q_\perp = 0$ and $q_\perp = \pi$ are not allowed between the $|t^+\rangle$ and $|t^0\rangle$ or $|t^0\rangle$ and $|t^-\rangle$). This is a remnant of the different type of geometries and the absence of “ladder-like” symmetries in the dimer case (see Appendix B).

Concerning the effective temperature in each model, the ladder remains more coherent in the low energy spectrum than the dimer since it “feels” a twice smaller temperature in unit of the effective dispersion. We discuss the low spectrum in more details in the next section (Sec. V) by comparing the results with field theory predictions.

Let us now turn to the higher part of the energy spectrum. This part of the spectrum is of course beyond the reach of the field theory and the mapping onto the anisotropic spin chain. As a general tendency we get weaker intensities and more spread signals when the temperature increases. The temperature leads also to a broadening of the modes, that was analyzed for the dimers from the numerical results.³⁴ We see here that the ladders show similar behavior in term of broadening. We concentrate here on the spectrum corresponding to an excitation to the state $|t^0\rangle$ and study in detail his temperature dependence, in particular for same order or larger temperature than the weak coupling (see Fig. 8). For both ladders and dimers, this part of the spectrum corresponds to modes in which a singlet or a $|t^+\rangle$ state is converted into a $|t^0\rangle$. One can thus examine this part of the spectrum as a single hole in a $t - J$ model¹⁸ for which the “hole” corresponds to the state $|t^0\rangle$ and the two “spin” states are played by the singlet and $|t^+\rangle$ states. At low (or zero) temperature as was clearly shown both for ladders at zero temperature (see Fig. 12,13 in 18) and for dimers (see Fig. 11,12 in 34) (note that the anti-symmetric signal $q_\perp = \pi$ is shifted by π in our results compared to the chain (in agreement with our Fig. 12)), the spectrum corresponds to two cosine dispersions centered around the two minima $q = \pi/2$ and $q = 3\pi/2$ because the creation of a $|t^0\rangle$ state is accompanied by the destruction of either a singlet $|s\rangle$ or a triplet $|t^+\rangle$ (see Sec. V.C.3.b in 18). At the magnetic field we have applied, the low part of the excited spectrum corresponds to the low energy states $|t^+\rangle$ and $|s\rangle$ with momentum for the excitations of $q = \pm\pi/2$ at half filling.

From our numerical results we can follow the dispersion of the $|t^0\rangle$ mode as the temperature increases from temperatures small compared to the effective dispersion to temperatures large compared to this dispersion. The results are shown in Fig. 8.

The lower temperature is clearly in agreement with

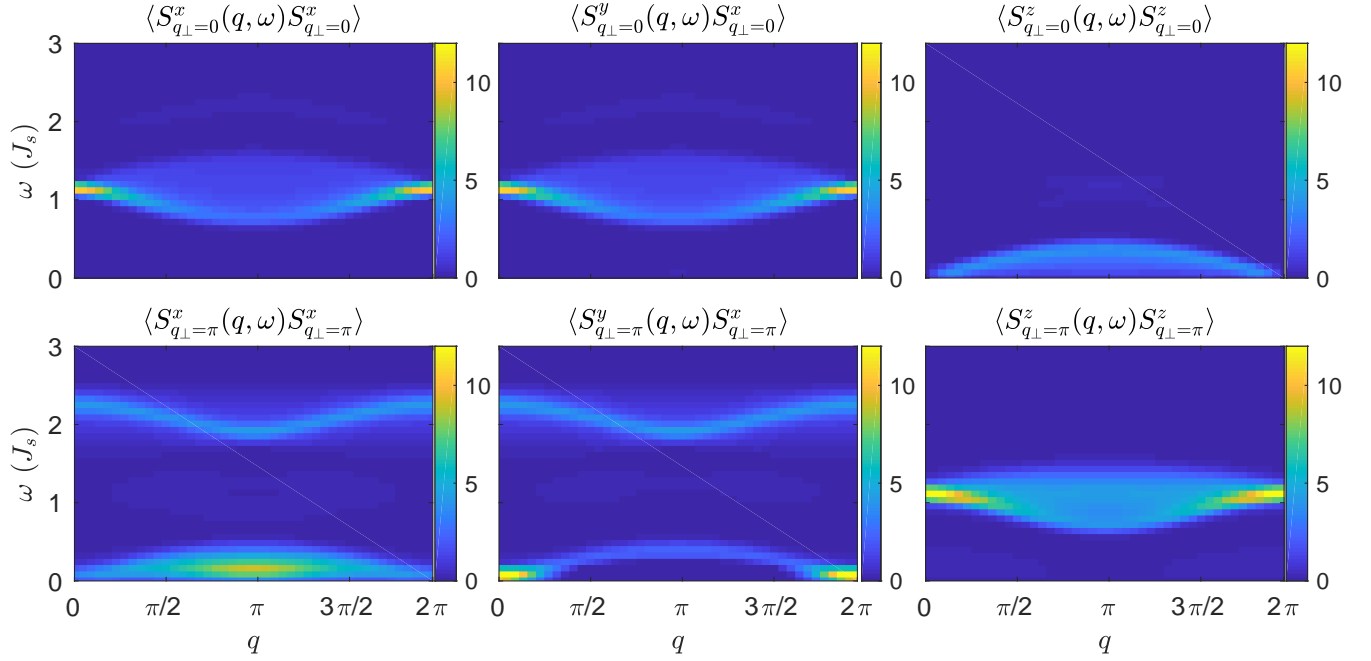


FIG. 5. Weakly coupled dimerized chain in units of $J_s = 1$ with $J_w = 0.39 J_s$ at $T = 0.25 J_s$ for magnetic field $h^z \simeq 1.148 J_s$ corresponding to $m_D = 0.25$. The resolution is $\delta\omega = \frac{\pi}{35 J_s^{-1}}$ using the standard scheme.

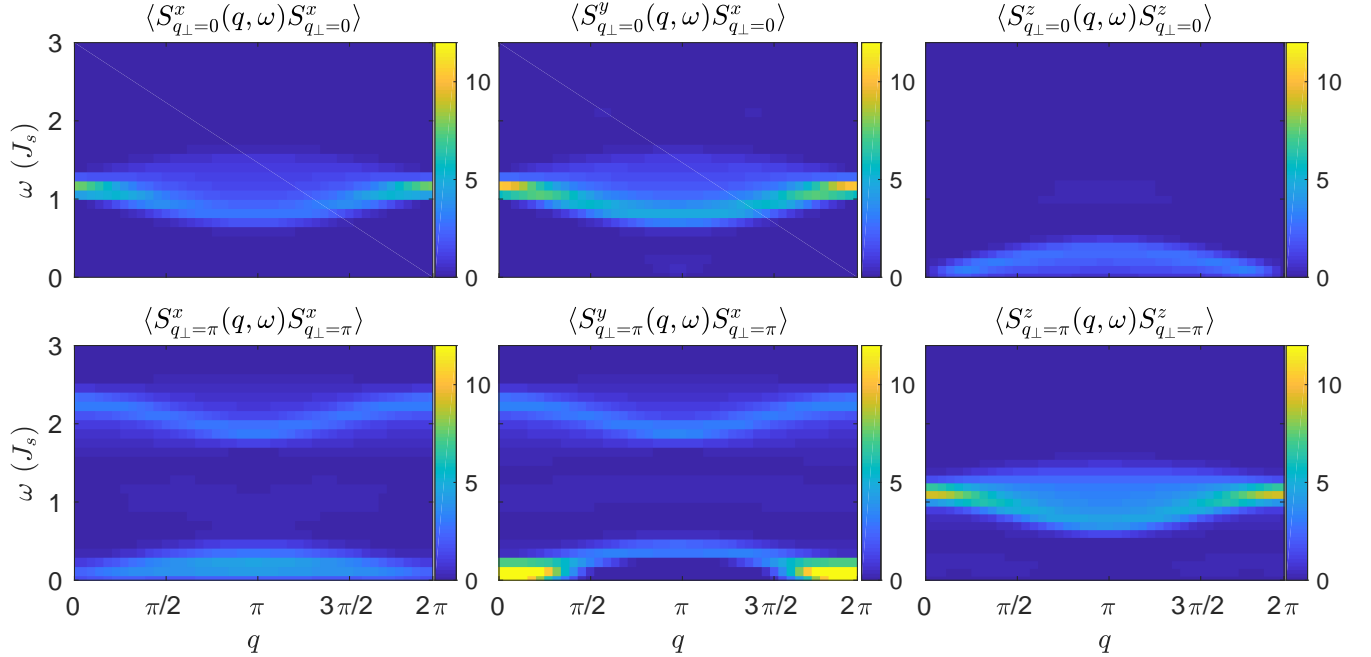


FIG. 6. Weakly coupled dimerized chain in units of $J_s = 1$ with $J_w = 0.39 J_s$ at $T \simeq 0.59 J_s$ for magnetic field $h^z \simeq 1.148 J_s$ corresponding to $m_D = 0.25$. The resolution is $\delta\omega = \frac{\pi}{27 J_s^{-1}}$ using the standard scheme.

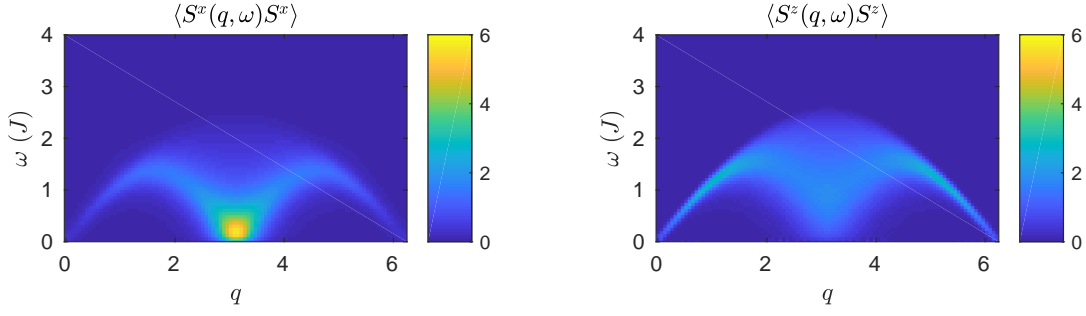


FIG. 7. XXZ spin-half chain with anisotropy $\Delta = \frac{1}{2}$ and coupling $J = 1$ at $T = 0.25 J$ for an external magnetic field $h = 0 J$ corresponding to a zero magnetization $m_c = 0$. The resolution is $\delta\omega = \frac{\pi}{52 J^{-1}}$.

the previous results both for the dimers and the ladders with the dispersion minima around $\pi/2$ and $3\pi/2$ resulting from the mapping to an effective $t - J$ model. As the temperature increases we see that the modes become increasingly incoherent and broaden. Quite surprisingly the numerical result shows that the dispersion leads to a strong intensity corresponding to a coherent like mode, with a strong intensity at the bottom of the spectrum, with a minimum which is now shifted to around $q \sim \pi$. This behavior is observed both for the dimers as shown in Fig. 8, but also for the ladders as can be seen from Fig. 4. Giving a precise description of this effective “mode” is an interesting challenging question. Although it is difficult to connect this observation directly to an analytical calculation, one can infer that the change of the spectrum comes from the fact that the “spinon” excitation that would correspond to the two pseudo spin states singlet $|s\rangle$ and triplet $|t^+\rangle$ are now essentially totally incoherent since the temperature is greater than their dispersion, leading to essentially the dispersion of the bare hole.

Note that this hole “band” is challenging to measure since it appears the strongest in the yx and not in the xx spin correlation which do not form such band so strongly. This weak signal process in the $\langle S^x(q, \omega) S^x \rangle_{q \perp=0}$ is actually compensated once the temperature starts populating the triplet zero $|t^0\rangle$ since there are as much negative energy transitions from $|t^0\rangle$ to $|s\rangle$ and $|t^+\rangle$ than positive transition from the $|s\rangle$ and $|t^+\rangle$ to $|t^0\rangle$. Polarized neutrons would be a priori required to extract this component.

V. COMPARISON WITH FIELD THEORY

Let us now turn to the low energy part of the spectra. Both the ladder and dimer system can be mapped^{18,34} at the *studied magnetic point* to an anisotropic spin-half $\Delta = \frac{1}{2}$ XXZ model. This allows to use the standard

bosonization method to extract the dynamical correlation functions⁴ both at zero temperature, and using the conformal invariance of the field theory, at low temperature. In a similar way than what was done for the NMR relaxation time³³ one can thus compare the numerical results with the field theory description.

A. Bosonization of the spin-half chain

Let us give a brief reminder of the field theory description. One introduces⁴ two continuous real bosonic fields ϕ and θ to represent the low energy excitations. For an XXZ spin chain, the effective Hamiltonian is

$$H = \frac{\hbar}{2\pi} \int dx \frac{uK}{\hbar^2} (\nabla\theta(x))^2 + \frac{u}{K} (\nabla\phi(x))^2 \quad (10)$$

where u is the velocity of excitations and K a dimensionless parameter, controlling the decay of the correlation functions. The spin operators are represented in term of the fields ϕ and θ by⁴

$$\begin{aligned} S^z(\mathbf{r}) &= m_z + \frac{-1}{\pi} \nabla\phi(\mathbf{r}) + \frac{2}{2\pi\alpha} \cos(2\phi(\mathbf{r}) - \pi(1 + 2m_z)x) \\ S^\pm(\mathbf{r}) &= \frac{e^{\mp i\theta(\mathbf{r})}}{\sqrt{2\pi\alpha}} (\cos(\pi x) + \cos(2\phi(\mathbf{r}) - 2\pi m_z x)) \end{aligned} \quad (11)$$

where m_z is the magnetization.

For ladders and dimerized chains, we use the spin-chain mapping described in Sec. II 3 to relate the observables to the ones of a spin chain.

$$\begin{aligned} S_l^z &= 2S_{l,k}^z - \frac{1}{2} \\ S_l^\pm &= (-1)^k \sqrt{2} S_{l,k}^\pm \end{aligned} \quad (12)$$

The spin-spin correlation functions are given in the retarded susceptibility form by^{4,47,48}

$$\chi_\kappa(\check{q}, \omega) = -\frac{\sin(\pi\kappa)\alpha^2}{u} \left(\frac{2\pi\alpha}{\beta u} \right)^{2\kappa-2} \text{B} \left(\frac{\kappa}{2} - i \frac{\beta(\omega - u\check{q} + i\varepsilon)}{4\pi}, 1 - \kappa \right) \text{B} \left(\frac{\kappa}{2} - i \frac{\beta(\omega + u\check{q} + i\varepsilon)}{4\pi}, 1 - \kappa \right) \quad (13)$$

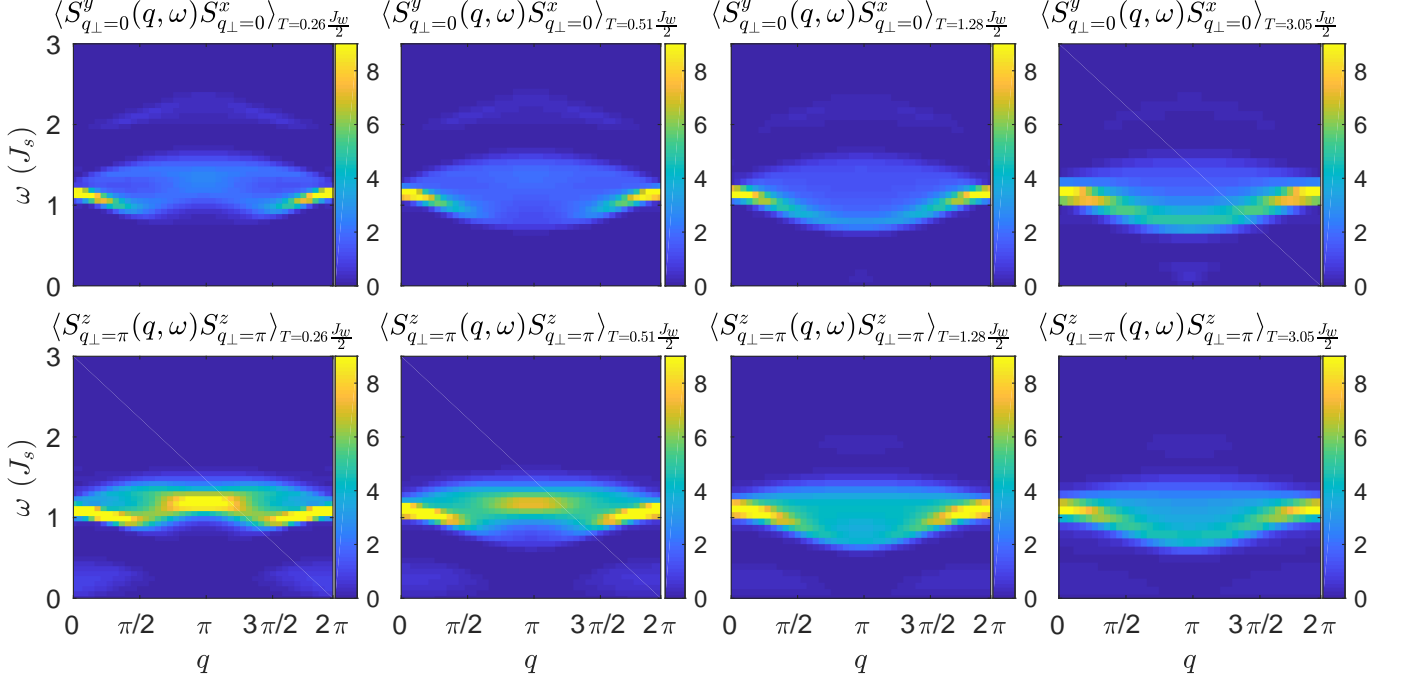


FIG. 8. Weakly coupled dimerized chain in units of $J_s = 1$ with $J_w = 0.39 J_s$. At the lowest temperatures we see that the minima of the dispersion are situated around $q = \pi/2$ and $q = 3\pi/2$ in agreement with the predictions of the mapping of this system to a $t - J$ model.¹⁸ When the temperature increases and becomes larger than J_w one sees that a coherent-like mode with a minimum around $q = \pi$ appears at the bottom of the spectrum (see text).

where β is the inverse temperature, the α is a short distance cutoff and \tilde{q} is the momentum centered on the field-dependent dispersion (the usual momentum q is defined in Sec. IV A 1). κ is an exponent that depends on the precise correlation function under consideration. In this paper we look at the *studied magnetic point* and on slices at $q = \pi$ so it would correspond to the $\tilde{q} = 0$ slice with TLL exponents $2\kappa = 2K$ or $2\kappa = \frac{1}{2K}$ according to equation (14).

The non-universal parameters of the field theory (TLL parameters and amplitudes for the correlation functions) can be computed directly allowing an essentially parameter free calculation of the correlation functions. For the spin chain with $\Delta = \frac{1}{2}$, exact Bethe-Ansatz results⁴⁹ fix $K = 0.75$ and $u = 1.299$. However, for the ladder and the dimer those parameters need to be fixed from a numerical calculation with the microscopic model.

B. Extraction of TLL parameters at $T = 0$

In order to fix the various parameters we use the expression of the correlation functions at zero temperature⁴

$$\begin{aligned} \langle S_i^x S_j^x \rangle &= (-1)^{|i-j|} A_x \left(\frac{1}{|i-j|} \right)^{\frac{1}{2K}} - B_x \left(\frac{1}{|i-j|} \right)^{2K + \frac{1}{2K}} \\ \langle \delta S_i^z \delta S_j^z \rangle &= \frac{-K}{2\pi^2} \left(\frac{1}{|i-j|} \right)^2 + A_z (-1)^{|i-j|} \left(\frac{1}{|i-j|} \right)^{2K} \end{aligned}$$

These expressions can then be used, by comparison with the numerical results, to extract^{18,50} the non-universal amplitudes A_x , B_x , A_z and the K parameter. We perform the zero temperature DMRG calculation of the correlation functions using the ALPS library.⁵¹

We first extracted the A_x and K parameter from the $\langle S_i^x S_j^x \rangle$ correlation since it has the slowest decay. We then use the obtained value of K in the $\langle S_i^z S_j^z \rangle$ correlation and fix A_z . We avoid boundary effects by considering correlations near the middle of the chain and by using space invariance for few sites in the bulk. With this procedure, we estimate all errors on the extracted values of about 20%. The velocity u is computed from the compressibility $\frac{K}{u\pi} = \frac{\partial m}{\partial h}$. In this work we used $u \simeq 1.3$. The

TABLE II. TLL parameters extracted from $T = 0$ DMRG data for chain, dimer and ladder systems. In italic A_z^C , could not be extracted directly from the DMRG, but has been fixed between the chain and the ladder (see text).

TLL parameters	chain \mathcal{C}	dimer \mathcal{D}	ladder \mathcal{L}
A_x	0.135	0.1469	0.166
B_x	0.021	0.0135	0.007
A_z	0.09	<i>0.082</i>	0.078
K	0.745	0.754	0.85

TLL values can be found in the table II and are consistent when they can be compared with previous results.^{18,50}

For the dimer system, it is more difficult than for the chain and the ladder to extract the TLL parameters. For instance, the $\langle S_i^z S_j^z \rangle$ correlation decreases very fast while on the other hand the local magnetization still oscillates. With the asymmetry in the correlation, it becomes difficult to extract from there any estimation of A_z^D . This particular value has thus been fixed to be between the chain and the ladder value.

C. Bosonization and T-DMRG comparison

Since we have now fixed all the non-universal TLL parameters and amplitudes from Table II, we can use the field theory expression (13) to obtain the correlation functions at finite temperature without any adjustable parameter. For the comparison between the direct numerical calculation of the correlations and the field theory, we consider the correlations at $q = \pi$ which are directly related to (D2) and (13) by

$$\begin{aligned}
 A_x \text{Im} \left(\chi_{\frac{1}{4K}}(\check{q} = 0, \omega) \right) &= \frac{1 - e^{-\beta\omega}}{-2} \langle \mathbb{S}^x(q = \pi, \omega) \mathbb{S}^x \rangle \\
 A_z \text{Im} (\chi_K(\check{q} = 0, \omega)) &= \frac{1 - e^{-\beta\omega}}{-2} \langle \delta \mathbb{S}^z(q = \pi, \omega) \delta \mathbb{S}^z \rangle
 \end{aligned} \tag{14}$$

The short distance cutoff α can be taken as equal to 1 inside the retarded susceptibility since it is reabsorbed in the non-universal amplitudes $A_x = \left(\frac{\alpha^{\frac{1}{2K}-1}}{4\pi a^{\frac{1}{2K}-1}} \right)$ and $A_z = \left(\frac{\alpha^{2K-2}}{a^{2K-2} 2\pi^2} \right)$ according to definition (11), where a is the lattice spacing unit cell.

Let us first compare the field theory prediction with the numerical calculations of the correlations for the anisotropic spin 1/2 chain. The result is shown in Fig. 9.

As can be seen from the slices 9, 10 and 11 the agreement is excellent both for the longitudinal and the transverse correlations, for temperatures up to $T \lesssim 0.5J$ for all frequencies up to $\omega \lesssim J$ at which one would expect in any case the field theory description to cease to be valid, irrespectively of the thermal effects. Note that

the frequency regime for which the field theory is valid is much broader than what was the case for the NMR relaxation time.³³ This is probably due to the fact that here we focus on a specific value of q (slice) for which massless modes down to zero energy exist, rather than perform a summation over all q modes. It also confirms that for a quite broad range of temperatures and frequencies, the conformal modification of the zero temperature correlations correctly gives the finite temperature behavior. At larger temperatures $T > 0.64J$ and above, deviations start to appear, even if the low energy part of the spectrum remains remarkably robust even at quite high temperatures. Note in particular the axis intensities in Fig. 9 that clearly show how well equation (13) predicts the low spectrum behavior.

Quite remarkably, a similar excellent agreement is found for dimer and ladder systems as respectively shown in Fig. 10 and Fig. 11.

The range of temperatures and frequencies for which the low energy effective theory works remarkably well is again quite broad. Both ladders and dimers also show an excellent agreement with the field theory prediction for frequencies up to the natural cutoff of the model, J_{\parallel} for the ladder, or $J_w/2$ for the dimer system. For the ladder although we can only reach the relatively high temperatures of more than half J_{\parallel} the field theory remains quite excellent up to frequencies of order $\omega \lesssim J_{\parallel}$.

This very robust behavior of the field theory description, in a broad range of frequencies and temperatures, up – and sometimes even beyond – the natural cutoff of the theory is of course directly relevant in the way we can trust the application of such theories for treating more complex realizations (such as e.g. coupled systems). This is of course especially important to tackle the physics of compounds with low enough magnetic exchanges, such that they can be manipulated by realistic magnetic fields. The drawback of such compound is of course that the natural scale of energies (e.g. in a neutron scattering experiment) or temperatures that one can reach is getting closer to the magnetic exchange.

VI. CONCLUSION

In this work, we computed using a time dependent density renormalization group technique (T-DMRG) the dynamical structure factor of a ladder system of spin 1/2, as a function of the energy, momentum and temperature. We use an optimal scheme for the implementation of the time evolution in order to be able to reach the necessary resolution for the ladder system. We focus on the intermediate magnetic field regime for which the magnetization per rung or per dimer is half of the saturation value and the system has massless excitation and a low energy part that can be mapped onto a Tomonaga-Luttinger liquid.

The results are indicated in Fig. 3 and Fig. 4. We compare these spectra with the one of dimerized systems and

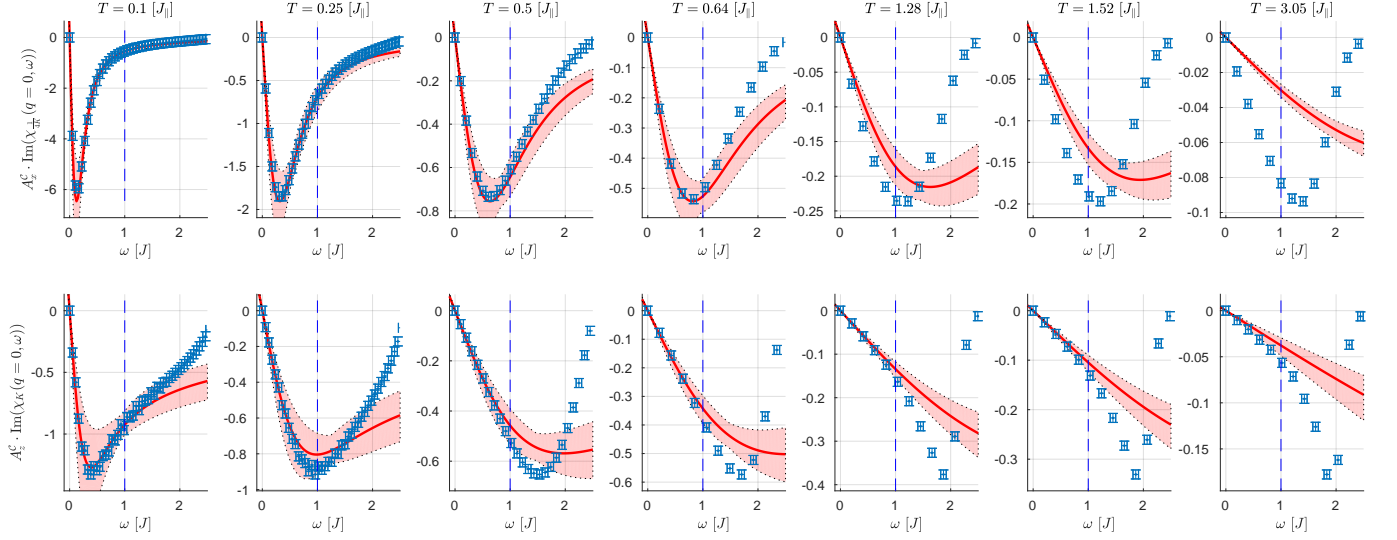


FIG. 9. Transverse (top) and longitudinal (bottom) spin-spin correlation functions for a chain of spin 1/2 as a function of the frequency ω for a fixed wavevector $q = \pi$, respectively $\tilde{q} = 0$ (see equation (14)). The field theory expression (13) in red is directly compared with the numerical T-DMRG calculation of the correlation (blue). The numerics are obtained from the Fourier transform of the output simulation without gaussian filter IV A 4. We have taken $A_x^C \simeq 0.135$, $A_z^C \simeq 0.09$ and $K^C \simeq 0.745$. The shadow region corresponds to the maximum and minimum of all TLL parameters moving by $\pm 10\%$.

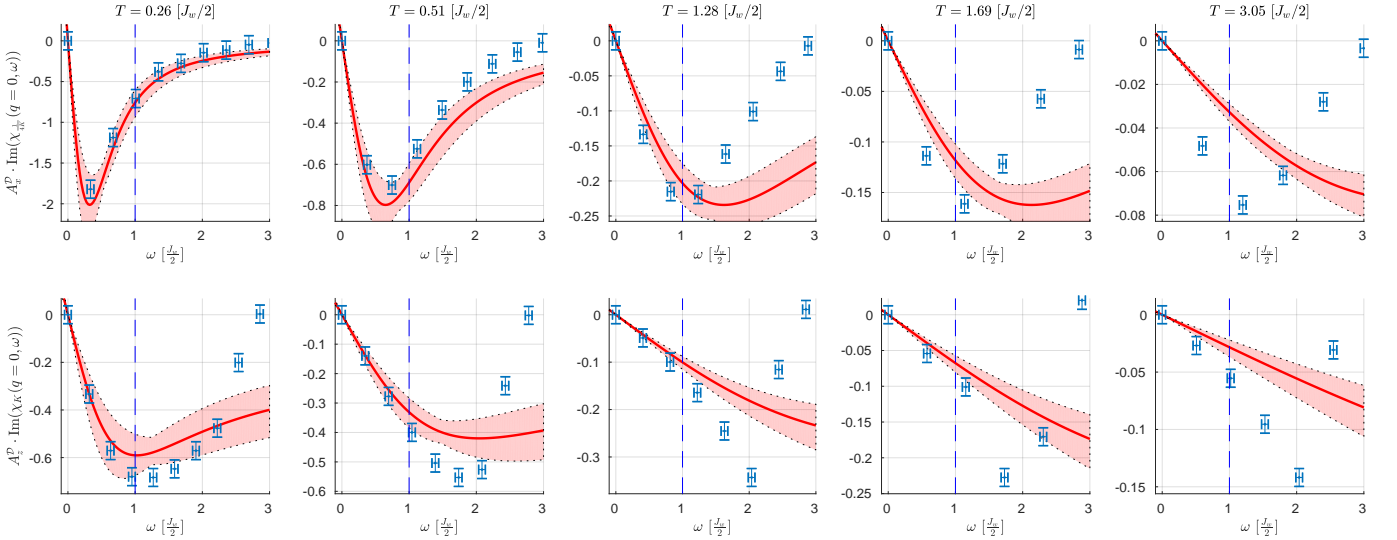


FIG. 10. Transverse (top) and longitudinal (bottom) spin-spin correlation functions for a dimerized chain as a function of the frequency ω for a fixed wavevector $q = \pi$, respectively $\tilde{q} = 0$ (see equation (14)). The field theory expression (13) in red is directly compared with the numerical T-DMRG calculation of the correlation (blue). The numerics are obtained from the Fourier transform of the output simulation without gaussian filter IV A 4. We have taken $A_x^D \simeq 0.1469$, $A_z^D \simeq 0.082$ and $K^D \simeq 0.754$. The shadow region corresponds to the maximum and minimum of all TLL parameters moving by $\pm 10\%$.

of anisotropic $\Delta = \frac{1}{2}$ XXZ chain, to which the low energy part of the previous systems can be mapped. We examine in particular the evolution of the intermediate energy part of the spectrum getting thermally populated by the triplet $|t^0\rangle$. For the low temperature part we examine the spin-chain mapping and compare the finite tempera-

ture correlations with the conformal modification of the TLL field theory. We show that there is an excellent agreement between the numerics and the field theory for energies and temperatures that extend up to values corresponding to the spin exchange of the weak coupling energy scale (J_{\parallel} for ladders and $J_w/2$ for dimers).

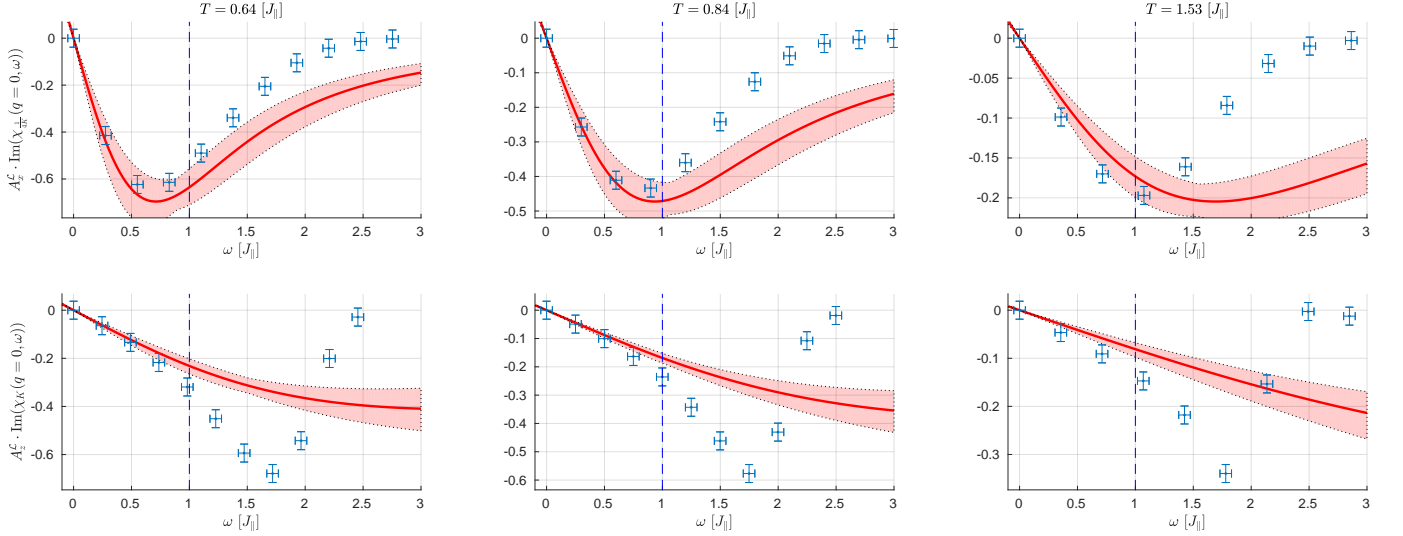


FIG. 11. Transverse (top) and longitudinal (bottom) spin-spin correlation functions for a ladder as a function of the frequency ω for a fixed wavevector $q = \pi$, respectively $\tilde{q} = 0$ (see equation (14)). The field theory expression (13) in red is directly compared with the numerical T-DMRG calculation of the correlation (blue). The numerics are obtained from the Fourier transform of the output simulation without gaussian filter IV A 4. We have taken $A_x^L \simeq 0.166$, $A_z^L \simeq 0.078$ and $K^L \simeq 0.85$. The shadow region corresponds to the maximum and minimum of all TLL parameters moving by $\pm 10\%$.

Our study shows clearly the direct possibility to use with an excellent accuracy the field theory description to study more complex systems of such ladders such as weakly 3D coupled ladders even if the temperature or the interladder coupling reaches reasonably strong values. It also shows that for systems as complex as the ladders we have an essentially exact description even at finite temperatures from the numerics and similar features can be found in related models (that we have already analyzed in that way) namely the spin chains and the dimerized systems.

Our calculation can potentially be directly confronted to measurements done with neutron scattering on ladder systems. Systems such as BPCB,⁵² DIMPY⁵³ and BPCC³⁸ are of course prime candidates for such a study. Very successful comparisons of the broad features of the neutrons have already been done with the zero temperature numerics. Our results open the door to a finer study of the temperature effects, or the study via numerics of the vicinity of quantum critical points in ladders for which such temperature effects are crucial to take into account.

ACKNOWLEDGMENTS

We thank C. Berthod, P. Bouillot, N. A. Kamar, S. Takayoshi, S. Ward and B. Wehinger for fruitful discussion. The calculation were done on the baobab and mafalda clusters. This work is partially supported by the Swiss National Science Foundation under Division II.

Appendix A: Dimer spectrum along the chain direction

The main text presents the results of the dimer (see Fig. 5) using the “ladder” representation (as shown in Fig. 1). For completeness and more easy comparison with Ref. 34 we also show in Fig. 12 the results along the chain geometry. The figure shows how the left-left cell

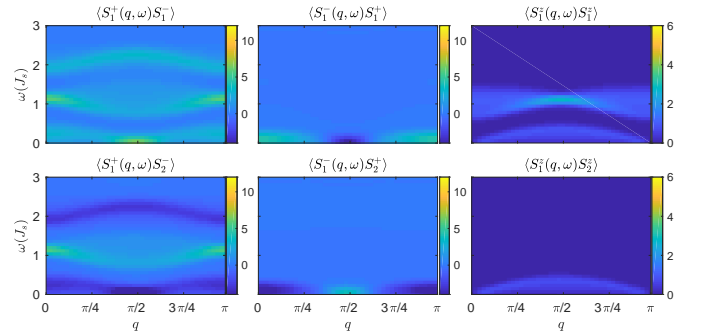


FIG. 12. Correlations along the chain of the weakly coupled dimerized chain at $T = 0.25 J_s$ with $J_w = 0.39 J_s$ and $J_s = 1$ for magnetic field corresponding to $m_D = 0.25$. Remark, that due to the geometry, the unit cells are now 2 sites periodic and the reciprocal space is π periodic.

$\langle S_1^\alpha(q, \omega) S_1^\gamma \rangle$ or left-right cell $\langle S_1^\alpha(q, \omega) S_2^\gamma \rangle$ disperse.

Appendix B: Symmetries in ladders and dimers

For the ladder, the rung and leg inversion symmetry for the middle cell rung $\ell_0 = \frac{N+1}{2}$ of an odd number of rung N ladder lead to

$$\begin{aligned} \langle S_{\eta_1, \ell}^\alpha(t) S_{\eta_2, \ell_0}^\gamma \rangle &= \langle S_{\eta_2, -\ell}^\alpha(t) S_{\eta_1, \ell_0}^\gamma \rangle = \\ \langle S_{\eta_2, \ell}^\alpha(t) S_{\eta_1, \ell_0}^\gamma \rangle &= \langle S_{\eta_1, -\ell}^\alpha(t) S_{\eta_2, \ell_0}^\gamma \rangle \end{aligned}$$

with $\eta_1, \eta_2 \in \{1, 2\}$. All correlations are space symmetric in the ℓ coordinate and we have equivalence between top-top and bottom-bottom correlations as well as bottom-top and top-bottom correlations. This makes the decomposition of the correlation in the $q_\perp \in \{0, \pi\}$ sectors appropriate.

For the dimer, there is only one rung or leg symmetry. For the middle rung cell $\ell_0 = \frac{N+1}{2}$ and for an odd number of rung, we have

$$\begin{aligned} \langle S_{1, \ell}^\alpha(t) S_{1, \ell_0}^\gamma \rangle &= \langle S_{2, -\ell}^\alpha(t) S_{2, \ell_0}^\gamma \rangle \neq \\ \langle S_{2, \ell}^\alpha(t) S_{2, \ell_0}^\gamma \rangle &= \langle S_{1, -\ell}^\alpha(t) S_{1, \ell_0}^\gamma \rangle \end{aligned}$$

The left-left and right-right correlations have same number of coupling met in both ℓ direction with reversed order (strong+weak vs weak+strong). They are pretty similar up to boundary effects.

The left-right and right-left correlations

$$\begin{aligned} \langle S_{1, \ell}^\alpha(t) S_{2, \ell_0}^\gamma \rangle &= \langle S_{2, -\ell}^\alpha(t) S_{1, \ell_0}^\gamma \rangle \neq \\ \langle S_{2, \ell}^\alpha(t) S_{1, \ell_0}^\gamma \rangle &= \langle S_{1, -\ell}^\alpha(t) S_{2, \ell_0}^\gamma \rangle \end{aligned}$$

are however very sensitive to the dimer geometry. For the first site correlations $\ell - \ell_0 \in \{-1, +1\}$, one crosses different amount of coupling in each direction (weak vs strong+weak). This asymmetry makes those correlations very sensitive to the dimerization structure even in the infinite size limit. For those reasons, the $q_\perp \in \{0, \pi\}$ is not a valid quantum number for the dimer even though there exist many similarities with the ladder.

Appendix C: Convergence and precision

Note first that we use the Suzuki-Trotter decomposition in the normalized units of the biggest energy scale to be consistent with the diverse numerical precision and matrix conditioning.

As a rule of thumb, we put the maximal bond dimension for the problem ($\chi_{\mathcal{L}} = 620$, $\chi_{\mathcal{D}} = 2400$). Of course, it costs much less computational resources to run the less consuming observables ($\frac{e^{-\beta H}}{\mathcal{Z}} S^-$ and $\frac{e^{-\beta H}}{\mathcal{Z}} S^z$, see Fig. 13) at smaller bond dimension χ . However, the artificial oscillation would start at different precision scales which we try to avoid. We always start with some maximal value χ and then, if needed, reduces the bond dimension to reach quicker the final resolution of the problem.

This gives full accuracy for the initial short time evolution which reduces the possibility of cumulative errors.

We present in Fig. 13 a plot of the bond dimension with the truncated weight ϵ_i (one step) of the Suzuki-Trotter process and the sum of all discarded weights $\sum_i \epsilon_i$ (integration) for three observables. The typically used mea-

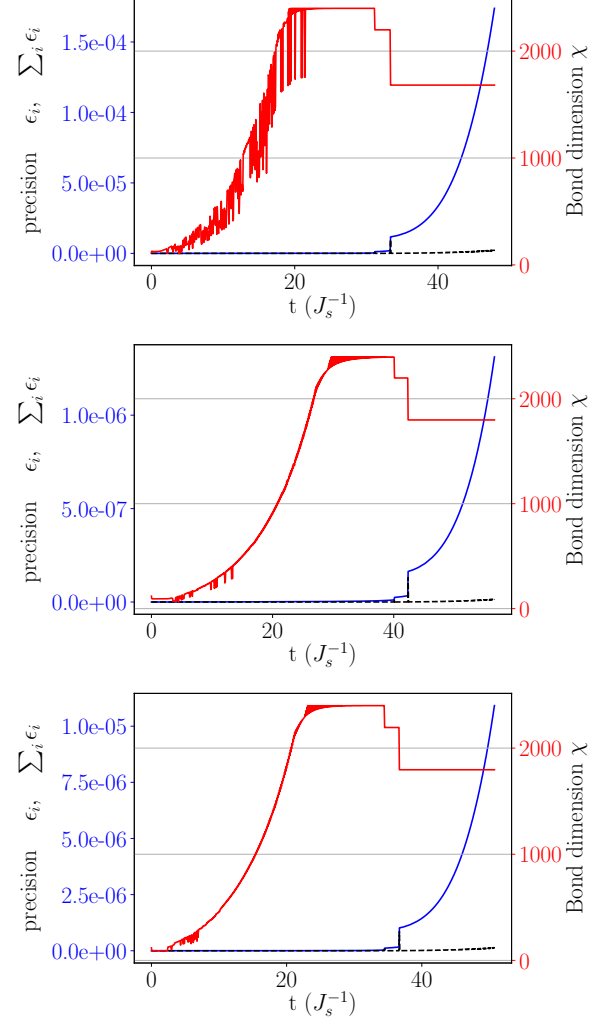


FIG. 13. Example on how the precision – truncated weight ϵ_i (dashed black line), sum of all discarded weight $\sum_i \epsilon_i$ (solid blue line) and bond dimension χ (red line) – grows with the time for three different observables $e^{+iHt} \frac{e^{-\beta H} S^\alpha}{\sqrt{\mathcal{Z}_{2\beta}}} e^{-iHt}$ in the ladder case at low temperature $\beta = 2\tilde{\beta} = 20.0 J_s^{-1}$. From top to bottom, we have α equal to “+”, “-” and “z”. The bond dimension truncation grows first until reaching 2400. The computation starting to be too heavy, we reduce it to 2200. Then after a computational time of the order of a few days we reduced it again to 1700 to reach reasonable computational times.

sure of errors in the simulation, namely the ϵ_i , is shown as the dashed black curve. In this work we however use the sum of all the discarded weights as the relevant error $\sum_i \epsilon_i$. We believe that this more stringent criteria helps

getting results which are more accurate and reproducible.

Appendix D: Lehmann representation and the detailed balance

The Lehmann representation consists of computing the averages using the exact eigenenergies E_n and eigenvectors $|n\rangle$ of the hamiltonian.

$$\langle A(t)B \rangle = \frac{1}{Z} \sum_{n,m} e^{-\beta E_n} e^{i(E_n - E_m)t} \langle n|A|m\rangle \langle m|B|n\rangle$$

It follows that the imaginary part of the susceptibility has the following symmetries

$$\text{Im}(\chi_{\text{ret}}^{\alpha\gamma}(q, \omega)) = -\text{Im}(\chi_{\text{ret}}^{\gamma\alpha}(-q, -\omega)) \quad (\text{D1})$$

due to

$$\begin{aligned} & -\frac{\pi}{Z} \sum_{n,m} (e^{-\beta E_n} - e^{-\beta E_m}) \langle n|S_{\frac{q}{2}}^{\alpha}|m\rangle \langle m|S_{-\frac{q}{2}}^{\gamma}|n\rangle \delta(\omega + E_n - E_m) = \\ & -\frac{\pi}{Z} \sum_{n,m} (e^{-\beta E_m} - e^{-\beta E_n}) \langle n|S_{-\frac{q}{2}}^{\gamma}|m\rangle \langle m|S_{\frac{q}{2}}^{\alpha}|n\rangle \delta(-\omega + E_n - E_m) \end{aligned}$$

The dynamical structure factor is related to the imaginary part of the susceptibility

$$S^{\alpha\gamma}(q, \omega) = \frac{-2}{1 - e^{-\beta\omega}} \text{Im}(\chi_{\text{ret}}^{\alpha\gamma}(q, \omega)) \quad (\text{D2})$$

due to

$$\begin{aligned} & -\frac{\pi}{Z} \sum_{n,m} (e^{-\beta E_n} - e^{-\beta E_m}) \langle n|S^{\alpha}|m\rangle \langle m|S^{\gamma}|n\rangle \delta(\omega + E_n - E_m) = \\ & \frac{(1 - e^{-\beta\omega})}{(-2)} \frac{(2\pi)}{Z} \sum_{n,m} e^{-\beta E_n} \langle n|S^{\alpha}|m\rangle \langle m|S^{\gamma}|n\rangle \delta(\omega + E_n - E_m) \end{aligned}$$

Thus the detailed balance equation follows from the two equations (D1) and (D2)

$$S^{\alpha\gamma}(q, \omega) = e^{-\beta\omega} S^{\gamma\alpha}(-q, -\omega) \quad (\text{D3})$$

-
- ¹ I. Bloch, J. Dalibard, and W. Zwerger, *Reviews of Modern Physics* **80**, 885 (2008) .
 - ² M. A. Cazalilla, R. Citro, T. Giamarchi, E. Orignac, and M. Rigol, *Reviews of Modern Physics* **83**, 1405 (2011) .
 - ³ A. Auerbach, *Interacting Electrons and Quantum Magnetism*, Graduate Texts in Contemporary Physics (Springer-Verlag, New York, 1994) .
 - ⁴ T. Giamarchi, *Quantum Physics in One Dimension*, International Series of Monographs on Physics (Oxford University Press, Oxford, 2003) .
 - ⁵ E. Dagotto and T. M. Rice, *Science* **271**, 618 (1996) .
 - ⁶ “Neutron Scattering in Condensed Matter Physics | Series on Neutron Techniques and Applications,” (2009) .
 - ⁷ C. Berthier, M. Horvatić, M.-H. Julien, H. Mayaffre, and S. Krämer, *Comptes Rendus Physique 2016 Prizes of the French Academy of Sciences /Prix 2016 de l’Académie des sciences*, **18**, 331 (2017) .
 - ⁸ J.-S. Caux and P. Calabrese, *Physical Review A* **74**, 031605 (2006) .
 - ⁹ B. Thielemann, C. Rüegg, H. M. Rønnow, A. M. Läuchli, J.-S. Caux, B. Normand, D. Biner, K. W. Krämer, H.-U. Güdel, J. Stahn, K. Habicht, K. Kiefer, M. Boehm, D. F. McMorrow, and J. Mesot, *Physical Review Letters* **102**, 107204 (2009) .
 - ¹⁰ B. Thielemann, C. Rüegg, K. Kiefer, H. M. Rønnow, B. Normand, P. Bouillot, C. Kollath, E. Orignac, R. Citro, T. Giamarchi, A. M. Läuchli, D. Biner, K. W. Krämer, F. Wolff-Fabris, V. S. Zapf, M. Jaime, J. Stahn, N. B. Christensen, B. Grenier, D. F. McMorrow, and J. Mesot, *Physical Review B* **79**, 020408 (2009) .
 - ¹¹ S. R. White, *Phys. Rev. Lett.* **69**, 2863 (1992) .
 - ¹² S. R. White, *Phys. Rev. B* **48**, 10345 (1993) .
 - ¹³ G. Vidal, *Phys. Rev. Lett.* **91**, 147902 (2003) .
 - ¹⁴ A. J. Daley, C. Kollath, U. Schollwöck, and G. Vidal, *Journal of Statistical Mechanics: Theory and Experiment* **2004**, P04005 (2004) .
 - ¹⁵ G. Vidal, *Phys. Rev. Lett.* **93**, 040502 (2004) .
 - ¹⁶ S. R. White and A. E. Feiguin, *Phys. Rev. Lett.* **93**, 076401 (2004) .
 - ¹⁷ U. Schollwöck, *Annals of Physics* **326**, 96 (2011), january 2011 Special Issue .
 - ¹⁸ P. Bouillot, C. Kollath, A. M. Läuchli, M. Zvonarev, B. Thielemann, C. Rüegg, E. Orignac, R. Citro, M. Klanjšek, C. Berthier, M. Horvatić, and T. Giamarchi, *Physical Review B* **83**, 054407 (2011) .
 - ¹⁹ D. Schmidiger, S. Mühlbauer, A. Zheludev, P. Bouillot, T. Giamarchi, C. Kollath, G. Ehlers, and A. M. Tsvelik, *Physical Review B* **88**, 094411 (2013) .
 - ²⁰ M. Klanjšek, H. Mayaffre, C. Berthier, M. Horvatić, B. Chiari, O. Piovesana, P. Bouillot, C. Kollath, E. Orignac, R. Citro, and T. Giamarchi, *Physical Review Letters* **101**, 137207 (2008) .
 - ²¹ D. Schmidiger, P. Bouillot, S. Mühlbauer, S. Gvasaliya, C. Kollath, T. Giamarchi, and A. Zheludev, *Physical Review Letters* **108**, 167201 (2012) .
 - ²² S. Sachdev, *Quantum Phase Transitions* (Cambridge University Press, 1999) .
 - ²³ S. Sachdev, T. Senthil, and R. Shankar, *Physical Review B* **50**, 258 (1994) .
 - ²⁴ F. Verstraete, J. J. García-Ripoll, and J. I. Cirac, *Phys. Rev. Lett.* **93**, 207204 (2004) .
 - ²⁵ M. Zwolak and G. Vidal, *Phys. Rev. Lett.* **93**, 207205 (2004) .
 - ²⁶ A. E. Feiguin and S. R. White, *Phys. Rev. B* **72**, 220401 (2005) .
 - ²⁷ T. Barthel, *New Journal of Physics* **15**, 073010 (2013) .
 - ²⁸ T. Barthel, U. Schollwöck, and S. R. White, *Physical Review B* **79**, 245101 (2009) .
 - ²⁹ D. Blosser, N. Kestlin, K. Y. Povarov, R. Bewley, E. Coira, T. Giamarchi, and A. Zheludev, *Physical Review B* **96**, 134406 (2017) .
 - ³⁰ J. Becker, T. Köhler, A. C. Tiegler, S. R. Manmana, S. Wes-

- sel, and A. Honecker, *Physical Review B* **96**, 060403 (2017) .
- ³¹ F. Lange, S. Ejima, and H. Fehske, *Physical Review B* **97**, 060403 (2018) .
- ³² E. S. Klyushina, A. C. Tiegel, B. Fauseweh, A. T. M. N. Islam, J. T. Park, B. Klemke, A. Honecker, G. S. Uhrig, S. R. Manmana, and B. Lake, *Physical Review B* **93**, 241109 (2016) .
- ³³ E. Coira, P. Barmettler, T. Giamarchi, and C. Kollath, *Physical Review B* **94**, 144408 (2016) .
- ³⁴ E. Coira, P. Barmettler, T. Giamarchi, and C. Kollath, *Physical Review B* **98**, 104435 (2018) .
- ³⁵ K. Damle and S. Sachdev, *Physical Review B* **57**, 8307 (1998) .
- ³⁶ D. Blosser, V. K. Bhartiya, D. J. Voneshen, and A. Zheludev, *Physical Review Letters* **121**, 247201 (2018) .
- ³⁷ S. Ward, P. Bouillot, H. Ryll, K. Kiefer, K. W. Krämer, C. Rüegg, C. Kollath, and T. Giamarchi, *Journal of Physics. Condensed Matter: An Institute of Physics Journal* **25**, 014004 (2013) .
- ³⁸ S. Ward, M. Mena, P. Bouillot, C. Kollath, T. Giamarchi, K. P. Schmidt, B. Normand, K. W. Krämer, D. Biner, R. Bewley, T. Guidi, M. Boehm, D. F. McMorrow, and C. Rüegg, *Physical Review Letters* **118**, 177202 (2017) .
- ³⁹ H. Ryll, K. Kiefer, C. Rüegg, S. Ward, K. W. Krämer, D. Biner, P. Bouillot, E. Coira, T. Giamarchi, and C. Kollath, *Physical Review B* **89**, 144416 (2014) .
- ⁴⁰ T. Tajiri, H. Deguchi, M. Mito, S. Takagi, H. Nojiri, T. Kawae, and K. Takeda, *Journal of Magnetism and Magnetic Materials Proceedings of the International Conference on Magnetism (ICM 2003)*, **272-276**, 1070 (2004) .
- ⁴¹ M. Suzuki, *Journal of Mathematical Physics* **32**, 400 (1991) .
- ⁴² R. McLachlan, *SIAM Journal on Scientific Computing* **16**, 151 (1995) .
- ⁴³ S. Singh, R. N. C. Pfeifer, and G. Vidal, *Physical Review B* **83**, 115125 (2011) .
- ⁴⁴ C. Hubig, I. P. McCulloch, and U. Schollwöck, *Physical Review B* **95**, 035129 (2017) .
- ⁴⁵ J. Eisert, M. Cramer, and M. B. Plenio, *Reviews of Modern Physics* **82**, 277 (2010) .
- ⁴⁶ O. Tange, *login: The USENIX Magazine* **36**, 42 (2011) .
- ⁴⁷ H. J. Schulz and C. Bourbonnais, *Physical Review B* **27**, 5856 (1983) .
- ⁴⁸ R. Chitra and T. Giamarchi, *Physical Review B* **55**, 5816 (1997) .
- ⁴⁹ T. Giamarchi and A. M. Tsvelik, *Physical Review B* **59**, 11398 (1999) .
- ⁵⁰ T. Hikihara and A. Furusaki, *Physical Review B* **63**, 134438 (2001) .
- ⁵¹ M. Dolfi, B. Bauer, S. Keller, A. Kosenkov, T. Ewart, A. Kantian, T. Giamarchi, and M. Troyer, *Computer Physics Communications* **185**, 3430 (2014) .
- ⁵² C. Rüegg, K. Kiefer, B. Thielemann, D. F. McMorrow, V. Zapf, B. Normand, M. B. Zvonarev, P. Bouillot, C. Kollath, T. Giamarchi, S. Capponi, D. Poilblanc, D. Biner, and K. W. Krämer, *Physical Review Letters* **101**, 247202 (2008) .
- ⁵³ D. Schmidiger, P. Bouillot, T. Guidi, R. Bewley, C. Kollath, T. Giamarchi, and A. Zheludev, *Physical Review Letters* **111**, 107202 (2013) .